

Three wave mixing vacuum squeezing generation in a SNAIL-based Traveling-Wave Parametric Amplifier with alternated flux polarity

Isita Chatterjee^{1,2}, Pegah Darvehi¹, Antonio Orsi^{1,2}, Anna Levochkina^{1,2},
 Pasquale Mastrovito^{2,1}, Gwenael Le Gal^{3,*}, Arpit Ranadive^{3,†}, Giulio Cappelli^{3,‡},
 Alberto Porzio⁴, Francesco Tafuri², Davide Massarotti^{5,1}, and Martina Esposito^{1,§}

¹ *CNR-SPIN Complesso di Monte S. Angelo, 80126 Napoli, Italy*

² *Dipartimento di Fisica “Ettore Pancini”, Università di Napoli “Federico II,” Monte S. Angelo, I-80126 Napoli, Italy*

³ *Université Grenoble Alpes, CNRS, Grenoble INP, Institut Néel, 38000 Grenoble, France*

⁴ *Dipartimento di Ingegneria Civile e Meccanica (DICEM),
 Università di Cassino e Lazio Meridionale, Cassino, Italy*

⁵ *Dipartimento di Ingegneria Elettrica e delle Tecnologie dell’Informazione,
 Università degli Studi di Napoli Federico II, via Claudio, I-80125 Napoli, Italy*

Recent demonstrations of squeezing generation using Traveling Wave Parametric Amplifiers (TW-PAs) have opened the way for the application of broadband microwave squeezing in quantum sensing, quantum-enhanced detection, and continuous-variable quantum information. Here we demonstrate vacuum squeezing generation via residual three-wave mixing (3WM) in a Josephson TWPA based on superconducting nonlinear asymmetric inductive elements (SNAILS) with alternated magnetic flux polarity. By investigating competition between four-wave mixing (4WM) and 3WM nonlinearities, we prove that vacuum squeezing generation via residual 3WM is possible when a careful choice of the operating flux point is adopted. Our study provides valuable insights on the impact of competing nonlinearities on TWPA squeezers, potentially extending the range of applications in the framework of microwave photonics.

I. INTRODUCTION

Squeezed states of the electromagnetic radiation play a central role in quantum technologies, since they allow noise reduction below the standard quantum limit (SQL) by redistributing quantum fluctuations among conjugate field quadratures [1]. While squeezing was initially extensively studied in the optical frequency domain, significant progress over the past decade in the field of superconducting quantum circuits has driven intense research efforts for squeezing generation in the microwave regime [2, 3]. Applications of microwave squeezing generation include, for example, quantum-enhanced detection [4–6], continuous-variable quantum information [7], quantum communication [8], and entanglement transfer protocols [9, 10].

Josephson-junction-based parametric amplifiers provide controllable nonlinearities that enable the generation of microwave squeezed states [11]. Early implementations of microwave squeezing relied on resonator-based Josephson parametric amplifiers (JPAs), showing remarkable squeezing performance with bandwidth typically limited to the range of 10-100 MHz [12–14].

To address the demand of broadband microwave squeezing generation, Josephson Traveling Wave Parametric Amplifiers (JTWPAs) have recently emerged as sources of non-classical microwave radiation, both in

3WM [15, 16] and 4WM [17, 18] regimes. However, the impact of competition between 3WM and 4WM nonlinearities on squeezing generation in TWPA devices has not yet been investigated.

Here, we report an experimental study of vacuum squeezing generation in a prototypical flux-tunable JTWPA based on superconducting nonlinear asymmetric inductive element (SNAIL) [19] unit cells with alternated magnetic flux polarity. Such a device was first introduced in the literature as a 4WM amplifier [20] and 4WM squeezer [18]. Subsequent investigations have shown that typical Josephson junctions’ fabrication imperfections can activate residual 3WM, allowing second harmonic generation [21] and dynamic phase matching amplification [22]. Here, we demonstrate for the first time that residual 3WM can also be used for squeezing generation, provided that competing 4WM nonlinear processes are mitigated via an appropriate choice of the magnetic flux operating point.

We study the influence of competing 4WM processes on squeezing generation, by performing 3WM phase-dependent gain, single-mode squeezing, and two-mode squeezing experiments for two significant flux operating points, eventually providing an experimental procedure to identify optimal flux bias points for 3WM vacuum squeezing performance. The demonstrated 3WM squeezing regime has the advantage of a large separation in frequency between the pump and the squeezed photons, allowing for straightforward filtering out of the pump and thus facilitating applications, for example, in the context of superconducting quantum networks.

* Currently at CEA, Leti, Grenoble, France

† Currently at Google Quantum AI, Santa Barbara, CA, USA

‡ Currently at Fondazione Bruno Kessler (FBK), Trento, Italy

§ Corresponding author: martina.esposito@cnr.it

II. FLUX TUNABILITY PRELIMINARY CHARACTERIZATION

The adopted device is a SNAIL-based JTWPA with alternated flux polarity throughout the transmission line, as shown in the sketch in Fig. 1(a). Each unit cell is composed of a SNAIL element and a capacitance to ground, C_g . Each SNAIL is a superconducting loop with three identical Josephson junctions with critical current I_C in one arm, and one smaller Josephson junction with critical current rI_C in the other arm. By using Taylor expansion, the current phase relation of a SNAIL (see Appendix A) can be approximated as

$$\frac{I(\phi^* + \phi)}{\tilde{\alpha}I_C} \approx \phi - \beta\phi^2 - \gamma\phi^3, \quad (1)$$

where ϕ^* is such that $I(\phi^*) = 0$, and the coefficients are defined as follows

$$\tilde{\alpha} = r \cos(\phi^*) + \frac{1}{3} \cos\left(\frac{\phi^* - \phi_{\text{ext}}}{3}\right), \quad (2)$$

$$\beta = \frac{1}{2} \left[r \sin \phi^* + \frac{1}{9} \sin\left(\frac{\phi^* - \phi_{\text{ext}}}{3}\right) \right] / \tilde{\alpha}, \quad (3)$$

$$\gamma = \frac{1}{6} \left[r \cos \phi^* + \frac{1}{27} \cos\left(\frac{\phi^* - \phi_{\text{ext}}}{3}\right) \right] / \tilde{\alpha}. \quad (4)$$

The coefficients β and γ are the 3WM and 4WM nonlinear coefficients respectively, while $\phi_{\text{ext}} = 2\pi\Phi_{\text{ext}}/\Phi_0$ is the reduced external magnetic flux, with $\Phi_0 = h/(2e)$ the magnetic flux quantum. Fig. 1(b) reports the flux-dependent behavior of β and γ for one SNAIL, considering the design parameter of the adopted device. Since the β coefficient is an odd function of the external flux, the alternated magnetic flux polarity configuration should ideally provide an overall suppression of 3WM processes at the TWPA output for wavelengths much larger than the unit cell size. However, as demonstrated in our previous study [21], Josephson junctions' fabrication imperfections can lead to a residual 3WM nonlinearity, which for example has been recently implemented for dynamic phase matching amplification [22]. In the following, we experimentally demonstrate that such residual 3WM nonlinearity can be employed for squeezing generation.

To identify suitable flux operating points for squeezing generation with residual 3WM, we perform a flux-dependent measurement of the generated idler power spectral density (PSD) with a spectrum analyzer, both in 3WM and 4WM configurations. The experimental results reporting the measured idler power referred at the TWPA output are shown in Fig. 2 (b).

The measurement is performed using the setup described in Appendix B, where the external magnetic flux is controlled by injecting DC current in a superconducting coil underneath the device. By applying a pump tone

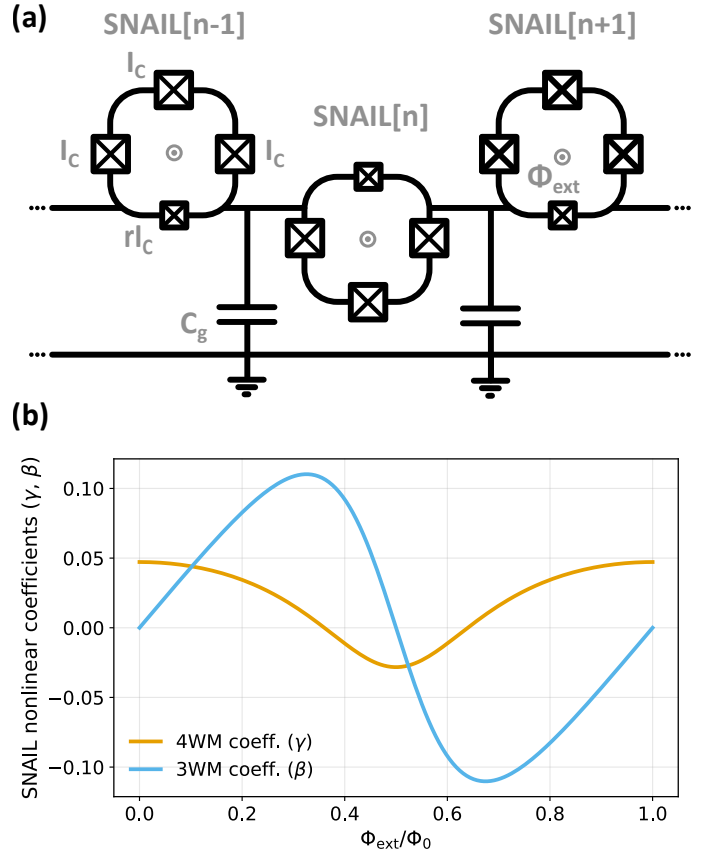


Figure 1. **Device sketch and SNAIL flux tunability.** (a) Circuit schematic of three neighboring unit cells in a SNAIL-based JTWPA device with alternated magnetic flux polarity. (b) 3WM coefficient β and 4WM coefficient γ for one SNAIL as a function of external magnetic flux.

at frequency f_p along with a signal tone at frequency f_s , we measure the power spectral density at the idler frequency $f_i = 2f_p - f_s$ (and $f_i = f_p - f_s$) for the 4WM (and 3WM) case as a function of the external flux. For the 3WM configuration, the signal is applied at $(f_p/2 - \Delta)$, while for the 4WM case the signal is applied at $(f_p - \Delta)$, where Δ indicates the frequency detuning. The pump frequency is kept the same for both cases. A sketch of the frequency configuration for 3WM and 4WM experiments is shown in Fig. 2 (a). The experimental results in Fig. 2 (b) are in qualitative agreement with WRSPICE transient simulations reported in Fig. 2 (c). The numerical simulations consider device parameters estimated in experimental characterizations [20], including also the typical Josephson junctions' fabrication imperfections (see Appendix C).

Based on the above characterization of the flux dependence of the nonlinearity, we identify two significant flux working points, both corresponding to about maximum values for the 3WM idler PSD (~ -130 dBm at TWPA output), but which significantly differ from the point of view of the 4WM idler PSD (~ 12 dB difference). The first identified flux point, $\Phi_1 = 0.59\Phi_0$, falls into a re-

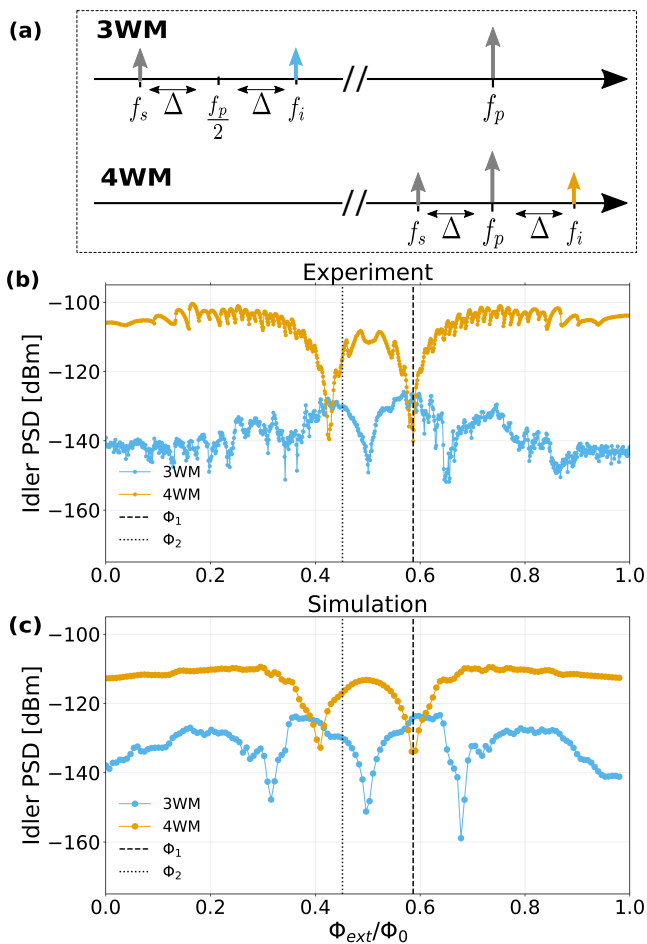


Figure 2. **Idler generation in 3WM and 4WM.** (a) Sketch of the frequency configuration for 3WM and 4WM experiments where $\Delta = 31$ MHz. (b) Experimental results for 3WM and 4WM idler measured power referred at TWPA output vs flux; pump frequency $f_p = 7.705$ GHz, pump power at device input $P_p = -87$ dBm, signal power at device input $P_s = -120$ dBm. (c) Results of WRSpice numerical simulations (see Appendix C). The vertical dashed and dotted lines indicate the selected flux points.

gion of maximum 3WM idler generation and minimum 4WM idler generation. In contrast, the second identified flux point, $\Phi_2 = 0.45 \Phi_0$, does not minimize the 4WM idler measured PSD. The two flux points are deliberately chosen to investigate the role of the combination of 3WM and 4WM nonlinearities on the squeezing generation in the regime of residual 3WM at the selected signal frequency. In the following, we report a comparative analysis of experimental results for phase-sensitive gain measurements, single-mode and two-mode squeezing experiments for these two selected working points.

III. GAIN AND SQUEEZING EXPERIMENTS

The experimental setup for gain and squeezing experiments is described in the Appendix B.

We first investigate the activation of residual 3WM parametric amplification by measuring the signal gain as a function of the pump phase in the degenerate configuration ($f_s = f_i = f_p/2$) for both the selected operating flux points. Specifically, we send at TWPA input a CW pump tone at frequency f_p along with a much weaker CW signal tone, locked in phase to the pump and measure the gain of the outgoing signal as a function of the input pump phase. In Fig. 3 (a) and (b) we report the experimental measure of phase-dependent 3WM gain for the two operating flux points for pump frequency $f_p = 7.705$ GHz, pump power $P_p = -84$ dBm for Φ_1 and $P_p = -91$ dBm for Φ_2 and signal power $P_s = -120$ dBm for both fluxes at the device input.

We observe significantly different results for the two flux points. For Φ_1 , in which 4WM idler generation is minimized, a phase-sensitive gain behavior is observed, as reported in Fig. 3 (a), showing a clear periodic amplification and de-amplification as expected for 3WM degenerate gain, proving the activation of an amplification process due to the residual 3WM nonlinearity. On the contrary, for the Φ_2 operating point, which has similar 3WM idler PSD as Φ_1 but 4WM idler PSD not minimized, the periodic amplification and de-amplification are not observed, as shown in Fig. 3 (b), suggesting a degradation of the degenerate 3WM gain due to competing 4WM processes.

To explore the role of competing nonlinearities specifically on the squeezing performance, we finally perform single-mode squeezing (SMS) and two-mode squeezing (TMS) experiments at the two selected flux points. Operationally, we drive the device with a CW pump tone at frequency f_p and fully reconstruct the quantum state generated at the TWPA output. To do so, we perform repeated acquisitions of the real and imaginary part of the output field quadratures at the frequencies of interest, that is $f_s = (f_p/2 - \Delta)$ and $f_i = (f_p/2 + \Delta)$, with $\Delta = 0$ for the SMS experiment, and $\Delta \neq 0$ for the TMS experiment. For each experiment, we acquire $N_{\text{rep}} \sim 10^6$ repeated acquisitions, each with an integration time of $10 \mu\text{s}$. We repeat the same experimental procedure for both pump ON and pump OFF.

We stress that as the field quadratures are measured at room temperature, the estimation of their values at the output of the TWPA requires normalization by the system gain, G_{sys} . We estimate G_{sys} by using a shot noise tunnel junction (SNTJ) as a reference noise source in a separated cooldown [23] (see Appendix D).

For Gaussian states, the covariance matrix encodes all the quantum properties of the state under investigation [24]. We estimate the covariance matrix of the quantum state at the output of the TWPA from the normalized experimental quadrature data. For the single mode case, we compute the covariance matrix for both pump OFF

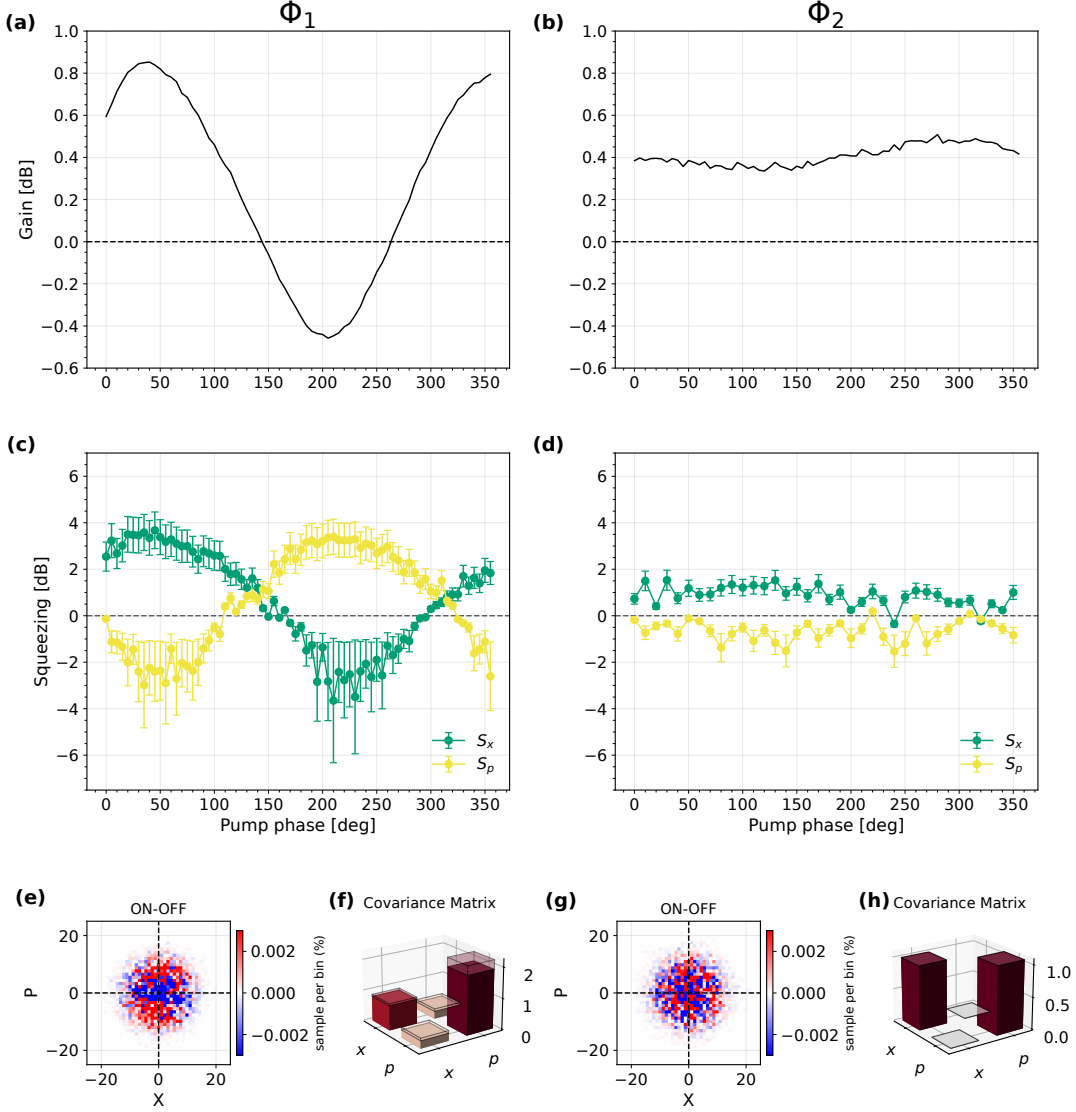


Figure 3. **Degenerate gain and single mode squeezing for Φ_1 (left) and Φ_2 (right).** (a-b) 3WM degenerate gain vs pump phase, pump frequency $f_p = 7.705$ GHz, pump power at TWPA input $P_p = -84$ dBm for Φ_1 and $P_p = -91$ dBm for Φ_2 . (c-d) 3WM single-mode squeezing values, S_x and S_p , along the x and p quadratures as a function of pump phase; number of repeated acquisitions for each phase, $N_{\text{rep}} = 3 \times 10^6$ for Φ_1 and $N_{\text{rep}} = 1 \times 10^6$ for Φ_2 ; integration time for each acquisition, $10 \mu\text{s}$. (e, g) Examples of single-mode differential (pump ON - pump OFF) phase space histogram plots for $N_{\text{rep}} = 8 \times 10^6$ repeated acquisitions and pump phase 220° and corresponding inferred covariance matrix with uncertainty indicated by shaded regions (f, h).

and pump ON as follows,

$$\sigma^{\text{meas}} = 4 \begin{pmatrix} \langle \hat{x}^2 \rangle - \langle \hat{x} \rangle^2 & \frac{1}{2} \langle \hat{x} \hat{p} + \hat{p} \hat{x} \rangle - \langle \hat{x} \rangle \langle \hat{p} \rangle \\ \frac{1}{2} \langle \hat{x} \hat{p} + \hat{p} \hat{x} \rangle - \langle \hat{x} \rangle \langle \hat{p} \rangle & \langle \hat{p}^2 \rangle - \langle \hat{p} \rangle^2 \end{pmatrix}, \quad (5)$$

where $\hat{x} = (\hat{a} + \hat{a}^\dagger)/2$ and $\hat{p} = (\hat{a} - \hat{a}^\dagger)/2i$ are the normalized single mode field quadratures operators, with \hat{a} and \hat{a}^\dagger the bosonic annihilation and creation operators such that $[\hat{a}, \hat{a}^\dagger] = 1$. Finally, we infer the covariance matrix of the quantum state $|\Psi\rangle$ generated at the output of the TWPA by subtracting the pump OFF noise background

as follows [25]

$$\sigma^{|\Psi\rangle} = \sigma^{\text{meas,ON}} - \sigma^{\text{meas,OFF}} + \mathbb{1}. \quad (6)$$

Note that we adopt a convention for field quadratures definition such that the covariance matrix for the vacuum state corresponds to the unit matrix.

Fig. 3(e) and (g) report examples of the differential (pump ON - pump OFF) phase-space histogram plot of single-mode quadrature experimental data for $N_{\text{rep}} = 8 \times 10^6$ repeated acquisitions for the operating flux Φ_1 and Φ_2 respectively, along with the corresponding inferred covariance matrix, Fig. 3(f) and (h). This experiment

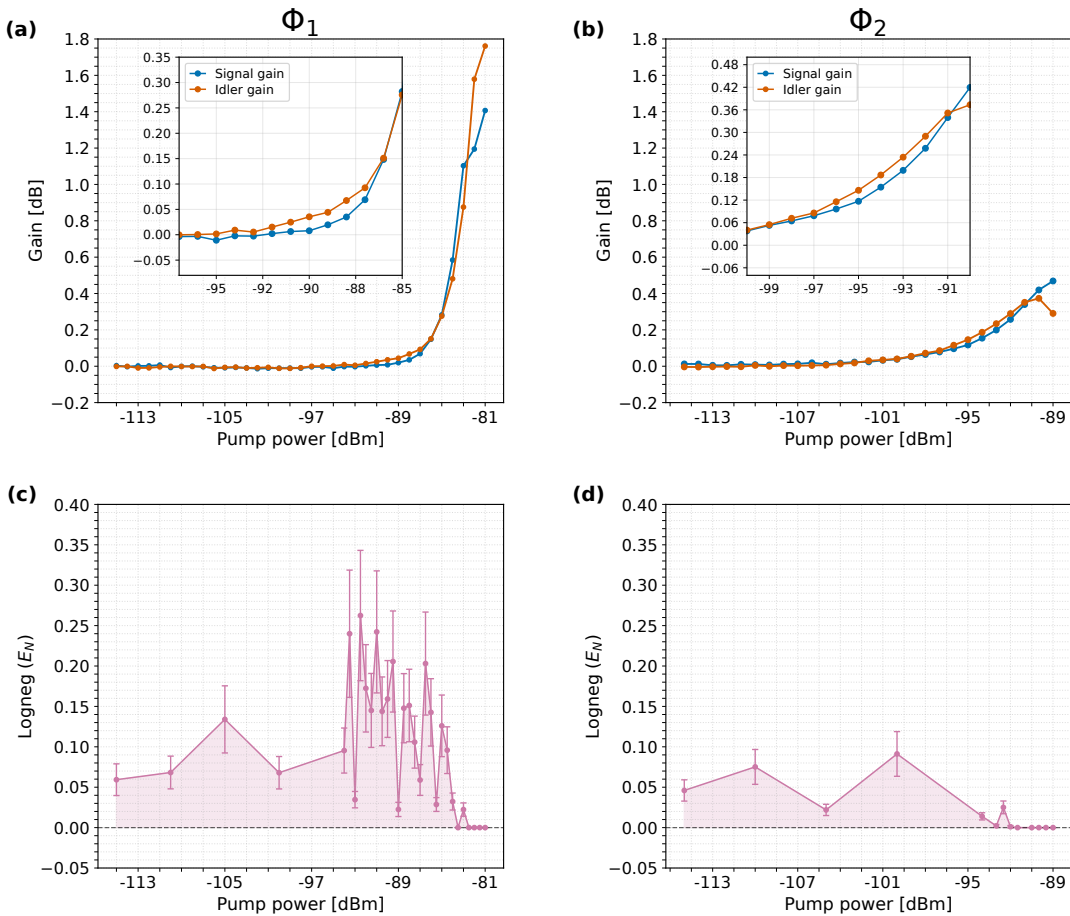


Figure 4. **Non-degenerate gain and entanglement verification in two-mode squeezing for Φ_1 (left) and Φ_2 (right).** (a-b) 3WM signal and idler gain experimental results versus pump power at TWPA input; the insets are zoom in of the results; pump frequency $f_p = 7.705$ GHz; detuning $\Delta = 31$ MHz for Φ_1 and $\Delta = 61$ MHz for Φ_2 . (c-d) Logarithmic negativity as a function of pump power; number of repeated acquisitions $N_{\text{rep}} = 1 \times 10^6$, integration time for each acquisition $10 \mu\text{s}$.

is repeated for different values of the input pump phase and the amount of squeezing, S_x and S_p , along the x and p quadratures, is estimated (see Appendix F details on how squeezing is computed from the covariance matrix). The results are shown in Fig. 3 (c) and (d) as a function of pump phase for both flux points. The pump powers are selected in order to have comparable maximum gain for the two operating flux points.

For the optimal flux point Φ_1 , our results demonstrate phase-dependent 3WM single-mode squeezing reaching maximum values of about 3 dB below the vacuum level. In contrast, for the flux point Φ_2 , no squeezing modulation is observed as a function of pump phase, proving the critical role of the operating flux choice for optimizing 3WM single-mode squeezing performance.

The results of the TMS experiments are reported in Fig. 4 and 5. For the TMS case, we pump the device with a CW tone at $f_p = 7.705$ GHz and perform N_{rep} repeated measurements of the real and imaginary part of the field quadratures at signal and idler frequency $f_s = f_p/2 - \Delta$ and $f_i = f_p/2 + \Delta$. We repeat the experiment for pump

ON and pump OFF and from the normalized quadrature data we compute the covariance matrix as follows,

$$\sigma_{mn}^{\text{meas}} = 4 \left[\frac{1}{2} \langle R_m R_n + R_n R_m \rangle - \langle R_m \rangle \langle R_n \rangle \right], \quad (7)$$

with $R = (\hat{x}_s, \hat{p}_s, \hat{x}_i, \hat{p}_i)$ the array of field quadratures operators including both signal and idler modes (see Appendix F). Finally, we infer the bipartite covariance matrix using Eq. (6).

The experiments and the associated estimation of the covariance matrix are repeated for different values of the input pump power. For each pump power we estimate the logarithmic negativity, defined as $E_N = \max[-\ln(\nu_-), 0]$, where ν_- is the smallest symplectic eigenvalue of the partially transposed covariance matrix (see Appendix F). According to the Positive Partial Transpose (PPT) criterion [26], the condition $E_N > 0$ is necessary and sufficient to demonstrate entanglement between the signal and idler modes.

The results for the TMS experiments versus pump power are reported in Fig. 4 for both operating flux

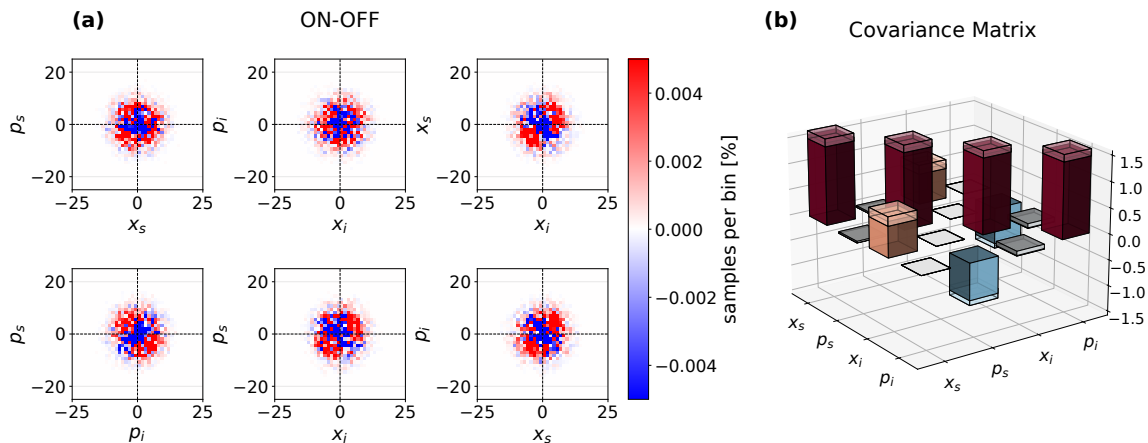


Figure 5. **Examples of two mode squeezing experimental results.** (a) Differential (pump ON - pump OFF) phase space histogram plots for $N_{\text{rep}} = 8 \times 10^6$ acquisitions with integration time $10 \mu\text{s}$. Flux operating point Φ_1 , pump frequency $f_p = 7.705$ GHz, detuning $\Delta = 31$ MHz, pump power at TWPA input $P_p = -83$ dBm. (b) Corresponding inferred covariance matrix with uncertainty signified by shaded region.

points. Panels (a-b) show the signal and idler gain, while panels (c-d) report the estimated logarithmic negativity for the bipartite state at the TWPA output. The detuning $\Delta = (f_i - f_s)/2$ is chosen to ensure symmetric gain for signal and idler modes [27].

In the low pump power regime (no TWPA gain), the logarithmic negativity is expected to be zero, corresponding to uncorrelated quadratures in the two-mode vacuum state. The observed non-zero values of E_N at low pump powers for both flux biases can be attributed to experimental artifacts, reported also in similar experimental demonstrations [15], such as drifts in the amplification chain occurring between the measurement sequences [28].

For the optimal flux point Φ_1 , as the pump power increases, we observe an increase of the logarithmic negativity with respect to the values in the low pump power regime, evidencing two-mode entanglement generation, followed by a decrease to zero values for higher pump powers. Fig. 5 shows an example of differential (pump ON - pump OFF) histogram plots of the two-mode experimental quadrature data and the corresponding reconstructed covariance matrix for the optimal flux point Φ_1 .

From results in Fig. 4(c), it is interesting to notice that the logarithmic negativity E_N approaches zero at high pump powers while the gain continues to increase. A similar behavior has been previously observed in TWPA squeezers [15, 18], suggesting the onset of pump-power dependent mechanisms responsible for entanglement degradation. A detailed study of this behavior is out of the scope of this work.

Finally, in contrast to the flux point Φ_1 where our results indicate two mode entanglement generation, for the flux point Φ_2 (results shown in Fig. 4(d)), the logarithmic negativity doesn't show any clear increase in the pump power range corresponding to similar gain values obtained for Φ_1 , denoting again a detrimental role

of competing 4WM processes on squeezing. Thus, our findings indicate that a preliminary optimization of the external magnetic flux working point aiming at minimizing the generation of 4WM idler is necessary in order to optimize 3WM single and two mode squeezing performance in flux tunable JTWPA.

IV. CONCLUSIONS

This work presents the first experimental demonstration of squeezing generation via residual 3WM in a SNAIL JTWPA with alternated flux polarity. Operating in the 3WM regime has the advantage of shifting the signal/idler band away from the pump frequency, allowing easy filtering of the pump and thus simplifying applications.

In addition to showing the versatility of Josephson metamaterials as TWPA squeezers, our work reports a detailed investigation on the impact of simultaneous activation of 3WM and 4WM nonlinearities on the squeezing performance.

We systematically investigate the residual 3WM regime versus the external applied magnetic flux and find that 3WM single and two-mode squeezing can be achieved provided that 4WM nonlinearity is carefully mitigated by an appropriate choice of the operating flux point.

Our results identify flux-bias control and competition between nonlinear mixing processes as key factors for squeezing performance, highlighting the need for optimization of these aspects in the design and operation of JTWPA squeezers.

ACKNOWLEDGMENTS

This project has received funding from the European Union under Horizon Europe 2021–2027 Framework Programme Grant Agreement No. 101080152, project TruePA, and under Horizon 2020 Research and Innovation Programme Grant Agreement No. 101017733, project “Superconducting quantum-classical linked computing systems (SuperLink)”, in the frame of QuantERA2 ERANET COFUND in Quantum Technologies”; and by Next Generation EU, Mission 4, NQSTI CUP B53C22004180005.

The authors thank Paolo Scotto Di Vettimo, CNR SPIN Naples, for his extensive technical assistance in setup preparation. The authors also thank Nicolas Roch and Luca Planat for insightful comments, and the QTLab group at University of Naples Federico II for helpful discussion. Finally, the authors thank Florent Lecocq and José Aumentado for providing the SNTJ and for useful comments.

DATA AVAILABILITY

The data that support the findings of this article are openly available on Zenodo id <https://doi.org/10.5281/zenodo.19701770>.

Appendix A: Device parameters and SNAIL unit cell

The adopted device was fabricated at the Nanofab facility of the Institut Néel, CNRS, in Grenoble. The fabrication process is nominally identical to the one described in [20], and it is based on a top-ground microstrip aluminum transmission line and Al-AlOx-Al Josephson junctions. The main circuit parameters, extracted from experimental characterizations [20], are listed in Table I.

Number of unit cells	700
Josephson capacitance, C_J	50 fF
Ground capacitance, C_g	250 fF
Critical current, I_c	2.19 μ A
SNAIL ratio, r	0.07

Table I. Circuit parameters for the adopted device [20].

The unit cells of the adopted JTWPA contain one SNAIL each, with alternated magnetic flux polarity throughout the chain. For a single SNAIL, considering the phase drop across the large Josephson junction as ϕ_L and across the small junction as ϕ , and by using the flux quantization for a single loop, we can write the difference between the phase drops across the lower and upper

branches of the superconducting loop as follows,

$$\phi - 3\phi_L = \phi_{\text{ext}}, \quad (\text{A1})$$

where $\phi_{\text{ext}} = 2\pi\Phi_{\text{ext}}/\Phi_0$ is the reduced external magnetic flux, with $\Phi_0 = h/(2e)$ the magnetic flux quantum. By using equation (A1), the current through each SNAIL element can be expressed as

$$I = rI_c \sin \phi + I_c \sin \left(\frac{\phi - \phi_{\text{ext}}}{3} \right). \quad (\text{A2})$$

By performing a Taylor expansion of I about ϕ^* such that $I(\phi^*) = 0$, we get the following approximated expression

$$\frac{I(\phi^* + \phi)}{I_c} \approx \left. \frac{\partial I}{\partial \phi} \right|_{\phi^*} \phi + \frac{1}{2} \left. \frac{\partial^2 I}{\partial \phi^2} \right|_{\phi^*} \phi^2 + \frac{1}{6} \left. \frac{\partial^3 I}{\partial \phi^3} \right|_{\phi^*} \phi^3, \quad (\text{A3})$$

that can be rewritten as in Equation (1) in the main text.

Appendix B: Experimental setup

A schematic of the experimental setup is shown in Fig. 6. The sample is anchored to the mixing chamber plate of a dilution refrigerator (*Triton*TM400 from Oxford Instruments). The external magnetic flux is controlled by injecting DC current in a superconducting coil placed alongside the device.

Two different cryogenic setups, in two separated cooldowns, have been adopted: one, including the TWPA, for the gain and squeezing experiments presented in the main text, and a second one, excluding the TWPA, for calibrating the system gain.

For the system gain calibration cooldown, the TWPA device is substituted with a shot noise tunnel junction (SNTJ) which is used as calibrated noise source. The adopted SNTJ has been fabricated by the team of José Aumentado and Florent Lecocq at NIST, Boulder, Colorado, USA [29]. A voltage bias can be applied to the SNTJ through a DC input line with low pass filter stages at room temperature, at the 4 K plate and at the mixing chamber plate.

At room temperature, two CW RF sources (R&S SGS100A and SGS100B) are used for generating the input pump tone at frequency f_p and signal tone at frequency f_s . A tunable phase shifter allows to control the pump phase.

For the experimental results reported in Fig. 2 at room temperature we measure the idler power spectral density (PSD) in dBm with a spectrum analyzer with set resolution bandwidth 3 kHz.

For the squeezing experiments, the output field quadratures are acquired using a room temperature microwave platform called Presto, from Intermodulation Products AB [30]. Such acquisition system does not require the use of analog mixers for down conversion and it easily enables the simultaneous detection of multiple frequency tones by assigning a single local oscillator (LO)

The normalization factor [15] is given by

$$v = \varepsilon \sqrt{\frac{\eta t_{\text{int}}}{G_{\text{sys}} Z_0 h f_{\text{acq}}}}, \quad (\text{D2})$$

where η indicates the internal loss of the TWPA device, G_{sys} is the estimated system gain, $Z_0 = 50 \Omega$ is the characteristic impedance of the microwave lines, h is Planck's constant, f_{acq} is the acquisition frequency, t_{int} is the integration time window, and $\varepsilon = 0.98$ is the calibrated Presto conversion coefficient which converts full scale (FS) units into Volts units.

Losses in the adopted JTWPA device are primarily arising from the dielectric losses in the capacitance to ground per unit cell, which is required for impedance matching. The insertion loss of the JTWPA is calculated from the dielectric loss tangent [34], $\tan \delta_0 = 2.1 \times 10^{-3}$, estimated from experimental characterizations [20, 32].

To estimate the system gain G_{sys} , we perform a separated cooldown in which we substitute the TWPA device with a shot noise tunnel junction (SNTJ) leaving the rest of the setup identical (see Fig. 6).

The noise power emitted by the SNTJ in the quantum regime ($k_B T \ll hf$) at frequency f as a function of the bias voltage V can be expressed as

$$N_{\text{SNTJ}}(f, V) = \left[\frac{1}{2} \left[\frac{eV + hf}{2k_B} \coth\left(\frac{eV + hf}{2k_B T}\right) + \frac{eV - hf}{2k_B} \coth\left(\frac{eV - hf}{2k_B T}\right) \right] + T_{\text{sys}} \right] \text{BW} G_{\text{sys}} k_B, \quad (\text{D3})$$

where BW denotes the measurement bandwidth.

We measure the power spectral density (PSD) recorded by a spectrum analyzer as a function of the bias voltage V applied to the SNTJ. We repeat this measurement for each of the frequencies of interest. For biasing, we use a filtered DC line with a 100 k Ω resistance at room temperature, which works as a voltage divider avoiding accidental blow-up [23]. We fit the obtained PSD to the noise model in Equation (D3) using three free parameters, the system gain, G_{sys} , the system noise temperature T_{sys} and the SNTJ electronic temperature T . Fig. 7 shows an example of measured power spectral density (PSD) as a function of the SNTJ bias voltage, along with the corresponding best-fit curve for a pair of frequencies signal/idler frequency tones.

We stress that the system gain obtained from the above method corresponds to the gain from the reference plane of the SNTJ to the input of the spectrum analyzer. The estimated system gains at the frequencies of interest are listed in Table II. We estimate an upper bound of 1 dB for the total insertion loss between the SNTJ output reference plane and the cryogenic isolator input reference plane, including loss from the SNTJ packaging and the used bias tee [35]. The G_{sys} value obtained from the SNTJ calibration is corrected by such upper bound

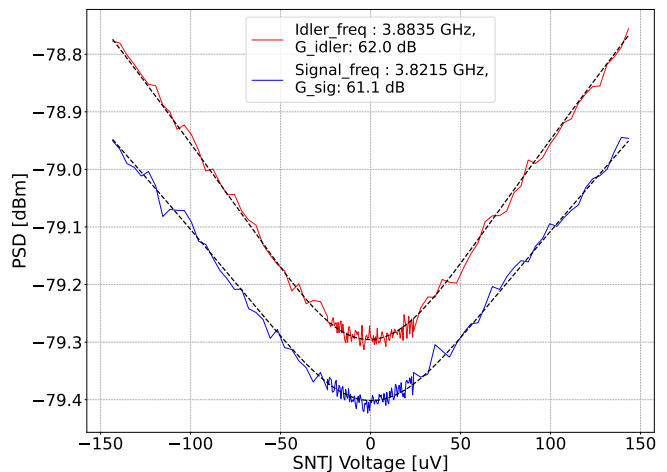


Figure 7. G_{sys} estimation using SNTJ. Example of measured PSD as a function of SNTJ voltage bias for a pair of signal and idler frequencies. Best fits are shown with dashed lines. G_{sys} best fit values are reported in the legend.

Acquisition frequency	G_{sys} [dB]
$f_p/2$	61.7
$f_p/2 + 31$ MHz	62.0
$f_p/2 - 31$ MHz	61.1
$f_p/2 + 61$ MHz	61.5
$f_p/2 - 61$ MHz	62.0
$f_p + 31$ MHz	46.5

Table II. Calibrated system gain for the different acquisition frequencies. $f_p = 7.705$ GHz.

loss estimation before it is used for the normalization of the quadrature data. This means that we use an upper bound estimation of G_{sys} and consequently a lower bound (conservative) estimation for squeezing and logarithmic negativity.

Considering the typical ripples in the insertion loss characterization of the microwave components between SNTJ and the isolator at mK temperature, we assume an uncertainty of 1 dB in our final estimation of G_{sys} . The error bars on the estimated covariance matrix and consequently on the estimation of squeezing and logarithmic negativity in this work are obtained assuming that the error on the G_{sys} estimation is the dominant one.

Appendix E: Estimation of the total input attenuation

The input pump and signal power reported in this work are all referred at the TWPA input. To do so we sum the power at the output of our RF source at room temperature to the total input line attenuation A_{in} , which indicates attenuation from the room temperature microwave sources to the input of the device at mK temperature.

The latter is estimated using the following formula,

$$S_{21}^{\text{off}} = A_{\text{in}} + \eta + G_{\text{sys}}, \quad (\text{E1})$$

where S_{21}^{off} is the transmission measured through the JTWPA when the pump is off, G_{sys} is the calibrated system gain, and η is the insertion loss of the TWPA in dB, estimated from the loss tangent, $\tan \delta_0 = 2.1 \times 10^{-3}$, obtained in experimental characterizations [20, 32]

Appendix F: Squeezing and Logarithmic negativity

The amount of single mode squeezing in dB along the x and p quadratures can be defined starting from the estimated single mode covariance matrix $\sigma^{|\Psi\rangle}$ (Eq. (6)) as follows,

$$S_x = 10 \log_{10} \left(\frac{\sigma_{11}^{|\Psi\rangle}}{\sigma_{11}^{(0)}} \right), \quad S_p = 10 \log_{10} \left(\frac{\sigma_{22}^{|\Psi\rangle}}{\sigma_{22}^{(0)}} \right). \quad (\text{F1})$$

With our convention for the field quadrature definition, the covariance matrix of the single mode vacuum state $\sigma^{(0)}$ correspond to the unity matrix. We use the definitions above to get the results in Fig. 3(c-d).

For the TMS, the main quantity of interest for the entanglement verification is the logarithmic negativity defined as,

$$E_N = \max[-\ln(\nu_-), 0], \quad (\text{F2})$$

where ν_- is the smallest symplectic eigenvalue of the partially transposed two-mode covariance matrix. This eigenvalue is given by,

$$\nu_- = \sqrt{\frac{\Delta\sigma - \sqrt{(\Delta\sigma)^2 - 4 \det \sigma}}{2}}, \quad (\text{F3})$$

$$\Delta\sigma = \det A + \det B - 2 \det C,$$

with A , B , and C denoting the submatrices of the two mode covariance matrix expressed in the following block structure,

$$\sigma = \begin{pmatrix} A & C \\ C^T & B \end{pmatrix}. \quad (\text{F4})$$

According to the Positive Partial Transpose (PPT) criterion [36, 37], a bipartite Gaussian state is separable only if the smallest symplectic eigenvalue of the partially transposed covariance matrix satisfies $\nu_- \geq 1$. Consequently, a sufficient condition for entanglement, is $\nu_- < 1$ or equivalently $E_N > 0$.

-
- [1] C. Fabre and N. Treps, Modes and states in quantum optics, *Reviews of Modern Physics* **92**, 035005 (2020).
- [2] X. Gu, A. F. Kockum, A. Miranowicz, Y.-x. Liu, and F. Nori, Microwave photonics with superconducting quantum circuits, *Physics Reports* **718-719**, 1 (2017).
- [3] M. Casariego, E. Zambrini Cruzeiro, S. Gherardini, T. Gonzalez-Raya, R. André, G. Frazão, G. Catto, M. Möttönen, D. Datta, K. Viisanen, J. Govenius, M. Prunnila, K. Tuominen, M. Reichert, M. Renger, K. G. Fedorov, F. Deppe, H. van der Vliet, A. J. Matthews, Y. Fernández, R. Assouly, R. Dassonneville, B. Huard, M. Sanz, and Y. Omar, Propagating quantum microwaves: towards applications in communication and sensing, *Quantum Science and Technology* **8**, 023001 (2023).
- [4] M. Malnou, D. Palken, B. Brubaker, L. R. Vale, G. C. Hilton, and K. Lehnert, Squeezed Vacuum Used to Accelerate the Search for a Weak Classical Signal, *Physical Review X* **9**, 021023 (2019).
- [5] K. M. Backes, D. A. Palken, S. A. Kenany, B. M. Brubaker, S. Cahn, A. Droster, G. C. Hilton, S. Ghosh, H. Jackson, S. K. Lamoreaux, *et al.*, A quantum enhanced search for dark matter axions, *Nature* **590**, 238 (2021).
- [6] L. Fasolo, A. Greco, E. Enrico, F. Illuminati, R. Lo Franco, D. Vitali, and P. Liveri, Josephson Traveling Wave Parametric Amplifiers as non-classical light source for Microwave Quantum Illumination, *Measurement: Sensors* **18**, 100349 (2021).
- [7] Y. Feng, G. Xu, X.-B. Chen, and Y. Guo, Microwave continuous-variable quantum key distribution in the open air, *Physical Review A* **111**, 042627 (2025).
- [8] S. Pogorzalek, K. G. Fedorov, M. Xu, A. Parra-Rodriguez, M. Sanz, M. Fischer, E. Xie, K. Inomata, Y. Nakamura, E. Solano, A. Marx, F. Deppe, and R. Gross, Secure quantum remote state preparation of squeezed microwave states, *Nature Communications* **10**, 2604 (2019).
- [9] J. Agustí, Y. Minoguchi, J. M. Fink, and P. Rabl, Long-distance distribution of qubit-qubit entanglement using Gaussian-correlated photonic beams, *Physical Review A* **105**, 062454 (2022).
- [10] A. Andrés-Juanes, J. Agustí, R. Sett, E. S. Redchenko, L. Kapoor, S. Hawaldar, P. Rabl, and J. M. Fink, Entangling remote qubits through a two-mode squeezed reservoir (2025), arXiv:2510.07139 [quant-ph].
- [11] J. Aumentado, Superconducting Parametric Amplifiers: The State of the Art in Josephson Parametric Amplifiers, *IEEE Microwave Magazine* **21**, 45 (2020).
- [12] S. Boutin, D. M. Toyli, A. V. Venkatramani, A. W. Edkins, I. Siddiqi, and A. Blais, Effect of Higher-Order Nonlinearities on Amplification and Squeezing in Josephson Parametric Amplifiers, *Physical Review Applied* **8**, 054030 (2017).
- [13] M. Malnou, D. Palken, L. R. Vale, G. C. Hilton, and K. Lehnert, Optimal Operation of a Josephson Parametric Amplifier for Vacuum Squeezing, *Physical Review Applied* **9**, 044023 (2018).

- [14] A. Bienfait, P. Campagne-Ibarcq, A. Kiilerich, X. Zhou, S. Probst, J. Pla, T. Schenkel, D. Vion, D. Esteve, J. Morton, K. Moelmer, and P. Bertet, Magnetic Resonance with Squeezed Microwaves, *Physical Review X* **7**, 041011 (2017).
- [15] M. Perelshtein, K. Petrovnin, V. Vesterinen, S. Hamedani Raja, I. Lilja, M. Will, A. Savin, S. Simbierowicz, R. Jabdaraghi, J. Lehtinen, L. Grönberg, J. Hassel, M. Prunnila, J. Govenius, G. Paraoanu, and P. Hakonen, Broadband Continuous-Variable Entanglement Generation Using a Kerr-Free Josephson Metamaterial, *Physical Review Applied* **18**, 024063 (2022).
- [16] A. Allocco, A. Celotto, E. Palumbo, B. Galvano, P. Livreri, L. Fasolo, L. Callegaro, and E. Enrico, Programmable Microwave Cluster States via Josephson Metamaterials (2025), arXiv:2507.22823 [quant-ph].
- [17] J. Y. Qiu, A. Grimsmo, K. Peng, B. Kannan, B. Lienhard, Y. Sung, P. Krantz, V. Bolkhovskiy, G. Calusine, D. Kim, *et al.*, Broadband squeezed microwaves and amplification with a josephson travelling-wave parametric amplifier, *Nature Physics* **19**, 706 (2023).
- [18] M. Esposito, A. Ranadive, L. Planat, S. Leger, D. Fraudet, V. Jouanny, O. Buisson, W. Guichard, C. Naud, J. Aumentado, F. Lecocq, and N. Roch, Observation of two-mode squeezing in a traveling wave parametric amplifier, *Phys. Rev. Lett.* **128**, 153603 (2022).
- [19] N. E. Frattini, U. Vool, S. Shankar, A. Narla, K. M. Sliwa, and M. H. Devoret, 3-wave mixing Josephson dipole element, *Applied Physics Letters* **110**, 222603 (2017).
- [20] A. Ranadive, M. Esposito, L. Planat, E. Bonet, C. Naud, O. Buisson, W. Guichard, and N. Roch, Kerr reversal in Josephson meta-material and traveling wave parametric amplification, *Nature Communications* **13**, 1737 (2022).
- [21] A. Y. Levochkina, H. G. Ahmad, P. Mastrovito, I. Chatterjee, G. Serpico, L. Di Palma, R. Ferroiuolo, R. Satariano, P. Darvehi, A. Ranadive, G. Cappelli, G. Le Gal, L. Planat, D. Montemurro, D. Massarotti, F. Tafuri, N. Roch, G. P. Pepe, and M. Esposito, Investigating pump harmonics generation in a SNAIL-based traveling wave parametric amplifier, *Superconductor Science and Technology* **37**, 115021 (2024).
- [22] A. Ranadive, B. Fazlaji, G. Le Gal, G. Cappelli, G. Butseraen, E. Bonet, E. Eyraud, S. Böhling, L. Planat, A. Metelmann, and N. Roch, A travelling-wave parametric amplifier isolator, *Nature Electronics* **8**, 1089 (2025).
- [23] M. Malnou, M. Vissers, J. Wheeler, J. Aumentado, J. Hubmayr, J. Ullom, and J. Gao, Three-Wave Mixing Kinetic Inductance Traveling-Wave Amplifier with Near-Quantum-Limited Noise Performance, *PRX Quantum* **2**, 010302 (2021).
- [24] G. Adesso, S. Ragy, and A. R. Lee, Continuous Variable Quantum Information: Gaussian States and Beyond, *Open Systems & Information Dynamics* **21**, 1440001 (2014).
- [25] E. Flurin, N. Roch, J. Pillet, F. Mallet, and B. Huard, Superconducting Quantum Node for Entanglement and Storage of Microwave Radiation, *Physical Review Letters* **114**, 090503 (2015).
- [26] P. Horodecki, Separability criterion and inseparable mixed states with positive partial transposition, *Physics Letters A* **232**, 333 (1997).
- [27] M. Houde, L. Govia, and A. Clerk, Loss Asymmetries in Quantum Traveling-Wave Parametric Amplifiers, *Physical Review Applied* **12**, 034054 (2019).
- [28] B. Jarvis-Frain, A. Schang, F. Quijandría, I. Nsanzineza, D. Dubyna, C. W. S. Chang, F. Nori, and C. M. Wilson, Observation of Genuine Tripartite Non-Gaussian Entanglement from a Superconducting Three-Photon Spontaneous Parametric Down-Conversion Source (2025), arXiv:2510.05405 [quant-ph].
- [29] M. Malnou, T. F. Q. Larson, J. D. Teufel, F. Lecocq, and J. Aumentado, Low-noise cryogenic microwave amplifier characterization with a calibrated noise source, *Review of Scientific Instruments* **95**, 034703 (2024).
- [30] M. O. Tholén *et al.*, Measurement and control of a superconducting quantum processor with a fully integrated radio-frequency system on a chip, *Rev. Sci. Instrum.* **93**, 104711 (2022), arXiv:2205.15253 [quant-ph].
- [31] A. Levochkina, Jtwp numerical simulations, https://github.com/levochkinanna/JTWP_Numerical_Simulations (2026).
- [32] A. Ranadive, *Nonlinear quantum optics with Josephson meta-materials*, Theses, Université Grenoble Alpes (2022), issue: 2022GRALY090.
- [33] A. Y. Levochkina, H. G. Ahmad, P. Mastrovito, I. Chatterjee, D. Massarotti, D. Montemurro, F. Tafuri, G. Pepe, and M. Esposito, Numerical Simulations of Josephson Traveling Wave Parametric Amplifiers (JTWPAs): Comparative Study of Open-Source Tools, *IEEE Transactions on Applied Superconductivity* **34**, 1 (2024).
- [34] L. Planat, E. Al-Tavil, J. P. Martínez, R. Dassonneville, F. Foroughi, S. Léger, K. Bharadwaj, J. Delaforce, V. Milchakov, C. Naud, O. Buisson, W. Hasch-Guichard, and N. Roch, Fabrication and Characterization of Aluminum SQUID Transmission Lines, *Physical Review Applied* **12**, 064017 (2019).
- [35] S.-W. Chang, J. Aumentado, W.-T. Wong, and J. C. Bardin, Noise measurement of cryogenic low noise amplifiers using a tunnel-junction shot-noise source, in *2016 IEEE MTT-S International Microwave Symposium (IMS)* (2016) pp. 1–4.
- [36] R. Simon, Peres-Horodecki Separability Criterion for Continuous Variable Systems, *Physical Review Letters* **84**, 2726 (2000).
- [37] G. Adesso and F. Illuminati, Gaussian measures of entanglement versus negativities: Ordering of two-mode Gaussian states, *Physical Review A* **72**, 032334 (2005).